Article

Photothermal skyrmion tweezer: programmable optical manipulation of magnetic topological quasiparticles

Jaeyu Kim[1,4], Seungmo Yang[2,4], Dongha Kim[1,3], Kyoung-Woong Moon[2], Changsoo Kim[2], Chanyong Hwang[2] ✉ & Min-Kyo Seo[1] ✉

Magnetic skyrmions, as topological quasiparticles, have shown great potential as information carriers for next-generation spintronic technologies, including memory, logic, and computing devices. While their non-trivial topological dynamics and interactions have been extensively explored, experimental control of individual skyrmions has so far relied mainly on global stimuli such as electric currents, magnetic fields, and surface acoustic waves. Efforts to achieve precise skyrmion positioning are significantly hampered by the skyrmion Hall effect and defect pinning. Here, we demonstrate high-precision trapping and transport of individual skyrmions using a photothermal potential well, thereby extending optical manipulation into the quasiparticle realm. Moreover, by integrating deterministic optical skyrmion creation and annihilation with photothermal and conventional electrical transport methods, we establish a fully programmable platform for systematic investigation of skyrmion dynamics and interactions. This approach opens new avenues towards reconfigurable and scalable architectures for future skyrmionic device applications and enriches studies of light–quasiparticle interactions in solid-state systems.

Magnetic skyrmions are topologically nontrivial quasiparticles characterized by a swirling spin configuration. Their robustness against external perturbations[1] and high electrical mobility under low current density[2] make skyrmions strong candidates for energy-efficient information carriers in memory devices, logics, and unconventional computing architectures[3–8]. Another distinctive feature of skyrmions is the emergent magnetic field originating from their topology, which gives rise to phenomena such as the skyrmion Hall effect[9,10] and the topological Hall effect[11,12]. Suppressing the skyrmion Hall effect[13–15] is necessary for efficient skyrmion transport; the topological Hall effect of electrons enables all-electrical skyrmion detection[16]. Recently, interactions of skyrmions with spin textures[17,18], magnons[19,20], and photons[21] have been reported, leading to various emergent phenomena analogous to particle–antiparticle interactions, Landau levels, and band structure reconstruction. Consequently, magnetic skyrmions provide a promising platform not only for demonstrating advanced spintronic devices but also for the study of rich dynamics and fundamental physics of topological quasiparticles.

Precise and programmable control of individual skyrmions is crucial both for systematic studies of their fundamental behavior and for the reliable operation of skyrmionic devices. Conventional electric current-driven techniques, however, face significant limitations: the applied current acts on multiple skyrmions simultaneously, reducing experimental selectivity and flexibility[22,23]. In addition, electrical transport and manipulation of magnetic skyrmions are constrained by the skyrmion Hall effect, which inherently deflects their trajectories[9,10], and defect pinning, which leads to unpredictable stochastic motion[24,25]. Alternative methods based on surface acoustic waves[26] or

[1]Department of Physics, KAIST, Daejeon, Republic of Korea. [2]Quantum Technology Institute, Korea Research Institute of Standards and Science, Daejeon, Republic of Korea. [3]Department of Physics, Korea University, Seoul, Republic of Korea. [4]These authors contributed equally: Jaeyu Kim, Seungmo Yang. ✉e-mail: cyhwang@kriss.re.kr; minkyo_seo@kaist.ac.kr

heat flow[27,28] present similar drawbacks. A recent approach utilizing a magnetic field gradient from a magnetic force microscopy probe[29] has demonstrated single-skyrmion manipulation, but it is constrained by slow operation speed and the inability to control and observe skyrmions simultaneously.

Optical tweezers, first demonstrated by Ashkin in 1986[30,31], use tightly focused laser beams to provide noncontact and precise control over physical objects, ranging from microspheres[32,33] and cells[34] to individual atoms[35,36], advancing research in biology[37], chemistry[33,38], and quantum sciences[39,40]. With optical tweezers, particle ensembles can be assembled on demand, enabling experiments from two-particle interactions[38,41] to many-body physics[42,43]. Extending such capabilities to emergent quasiparticles is therefore a natural and timely pursuit. To date, optical trapping and transport have been experimentally realized for magnetic bubbles in relatively thick magnetic films[44] and for Abrikosov vortices in superconductors[45]. For magnetic skyrmions, however, optical tweezing has so far remained theoretical, requiring extremely localized optical fields and strong magnetoelectric coupling[46]. Other theoretical works have explored skyrmion manipulation using moving traps or tips, as well as skyrmion dynamics in periodic or disordered pinning landscapes[47–49]. Aside from optical tweezing, another line of research, optical generation of skyrmionic textures, has recently been demonstrated[50–52]. Although ultrafast laser heating produces multiple skyrmions simultaneously, their number and position are determined stochastically. Achieving programmable creation and control of individual skyrmions would extend the well-established paradigm of optical tweezers to topological quasiparticles, establishing a powerful new platform for controlled studies of spin textures.

In this work, we introduce optical manipulation of skyrmions, magnetic topological quasiparticles in a spin system, and demonstrate their unique advantages. A micron-scale photothermal potential well, induced by focused laser incidence, enables precise two-dimensional tweezing and isolation of individual skyrmions, even overcoming the spin–orbit torque generated by electric current pulses. Beyond the reach of conventional optical tweezers, this photothermal approach enables deterministic creation and annihilation of individual skyrmions. By integrating this optical control with electrical transport, we establish fully programmable manipulation of skyrmions in two dimensions, providing a versatile platform for systematic studies of skyrmion dynamics and interactions, and opening new avenues toward reconfigurable architectures for quantum spintronic applications.

Results

Photothermal trap for spin textures

The core of our optical manipulation approach of individual skyrmions is a micrometer-scale photothermal potential well generated by focused laser incidence (Fig. 1a). In magnetic systems with the presence of the interfacial Dzyaloshinskii–Moriya interaction (DMI) and the perpendicular magnetic anisotropy (PMA), the energy density of a chiral domain wall (DW) can be expressed as[53,54] $U = 4\sqrt{AK_{eff}} - \pi D + \frac{\ln 2}{\pi}\mu_0 M_s^2 d$. Here, A is the exchange stiffness, K_{eff} is the effective PMA energy density per volume, D is the DMI energy density per surface, M_s is the saturation magnetization, and d is the film thickness. As the temperature increases, thermal fluctuations disrupt magnetic ordering, reducing key magnetic parameters[55]. According to Bloch's law, the saturation magnetization M_s decreases as the temperature approaches the Curie temperature, whereas A scales as[55] M_s^2. Similarly, both K_{eff} and D decrease due to thermal agitation[56,57]. Consequently, while the DMI energy density ($-\pi D$) increases, all other contributions to total energy density decrease in total energy density with temperature. By measuring K_{eff} and M_s as a function of temperature, we confirmed that the dominant factor driving the reduction in total energy density is the decrease in K_{eff} (Supplementary Note 1).

A focused laser with a Gaussian beam profile locally heats the magnetic medium, producing a Gaussian temperature distribution
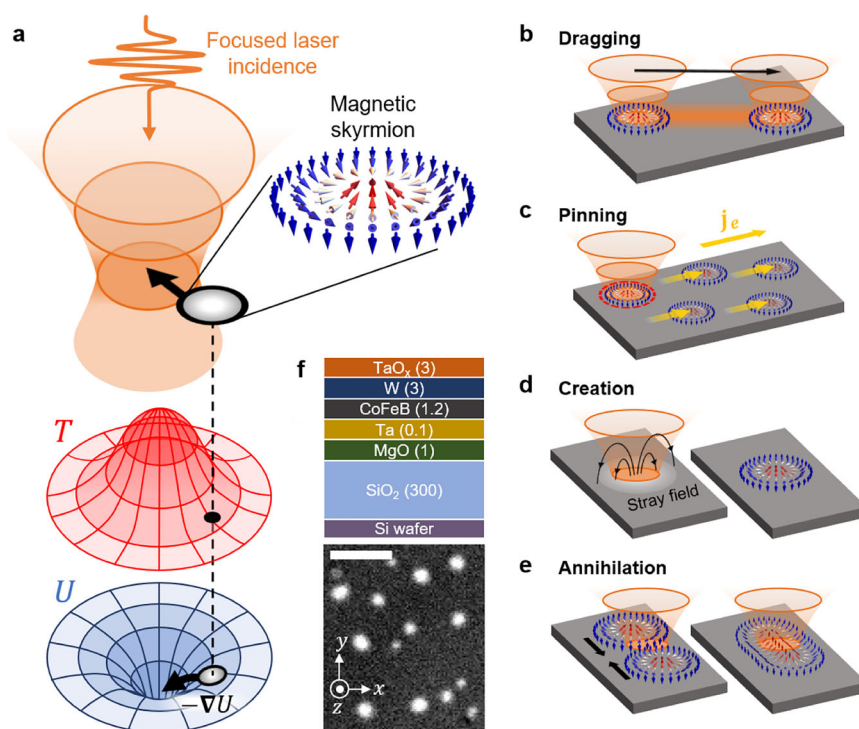

Fig. 1 | Photothermal manipulation of individual magnetic skyrmions.
a Illustration of the temperature (T) and potential energy (U) distributions created by the photothermal effect of focused laser incidence on the magnetic film. **b**–**e** Schematics of the photothermal dragging, pinning, creation, and annihilation of an individual skyrmion. **f** Top: Structure of the employed magnetic film, with the numbers in parentheses indicating the thickness of each layer in nanometers. Bottom: Magneto-optical Kerr effect microscope (MOKE) image of spontaneously generated magnetic skyrmions. Scale bar, 10 μm.

that forms a photothermal potential well, as confirmed by finite element simulations (see Supplementary Note 2 for details). Skyrmion dynamics within this photothermal potential can be described by the Thiele equation, where the anisotropy gradient induced by local heating serves as the driving force (see Supplementary Note 3). By steering the laser beam, individual skyrmions can be selectively dragged to desired locations or pinned at a specific site, effectively counteracting motion induced by electric currents (Fig. 1b, c). We note that thermomagnetic torques arising from thermal gradients may also influence skyrmion motion[27], but their contribution is typically weaker than that of the photothermal potential[58,59].

The photothermal effect induced by a high-intensity laser provides another opportunity to engineer individual skyrmions, enabling their selective creation or annihilation (Fig. 1d, e). When local heating exceeds a certain threshold temperature, the irradiated region undergoes demagnetization. Because the heated area has much reduced coercivity, the local magnetization flips due to the small stray field from the surrounding magnetic domains and stabilizes into a skyrmion. Moreover, by bringing one skyrmion close to another with our photothermal tweezer, we can induce contact between their DWs, causing them to merge into a single skyrmion. The size and shape of the merged skyrmion then rapidly relax to those characteristic of the host magnetic medium.

In this work, we examined skyrmions in a multilayer stack comprising MgO (1 nm)/Ta (0.1 nm)/$Co_{20}Fe_{60}B_{20}$ (1.2 nm)/W (3 nm)/TaO_x (3 nm) on a Si/SiO_2 substrate (for further details, see the "Methods" section). The Ta layer was introduced to finely tune the PMA, while the W/CoFeB interface generates DMI strong enough to stabilize the skyrmionic textures. The W layer also supports spin–orbit torques for electric current-driven manipulation of skyrmions. A magneto-optical Kerr effect (MOKE) microscopy setup was used to visualize magnetization states in real time, where dark and light regions correspond to magnetization along the −z and +z directions, respectively.

A small perpendicular magnetic field of 2.56 Oe was applied to optimize the size and density of skyrmions. The resulting skyrmion diameter ranged from 2.0 to 5.0 µm, making them clearly resolvable under an optical microscope. The MOKE image (Fig. 1f) reveals sufficiently well-separated skyrmions, allowing individual manipulation without interference from neighboring skyrmions. A skyrmion Hall

effect measurement confirms the topological nature of our magnetic textures, validating them as magnetic skyrmions (Supplementary Note 4).

Skyrmion tweezers

We first demonstrate the use of the photothermal tweezer for dragging a single magnetic skyrmion along the laser beam's sweep direction (Fig. 2a). Once a single skyrmion is trapped within the beam spot by the photothermal potential, we move the sample relative to the fixed laser position, and then, the skyrmion is transported accordingly. This functionality enables precise control over the arrangement of skyrmions, enabling the creation of arbitrary patterns of skyrmions (Fig. 2b). The potential well landscape resulting from the temperature gradient is universal for any spin textures, regardless of their detailed distributions, as long as the PMA energy remains dominant. As a result, we can control magnetic DWs, not just individual skyrmions (Supplementary Note 5). From a topological perspective, a chiral DW with a semicircular shape carries a topological charge of ±1/2, often referred to as a "half skyrmion"[60,61]. We can extract a half skyrmion not only from bulk domain structures but also from a single skyrmion, by selectively dragging one of its ends (Supplementary Note 5).

The probability of stable skyrmion transport, defined as the likelihood that a target skyrmion remains intact without elongation or pinning to a local defect, was measured by varying the sweeping speed (v_{sw}) and laser beam power (Fig. 2c). Strong local material defects can pin or deform skyrmions during photothermal tweezing. For each combination of sweeping speed and laser beam power, we conducted 20 trials and recorded the success probability of transporting a single skyrmion over a distance of 10 µm. At a sweeping speed of 120 nm/s and a laser power of 6.02 mW, we were able to drag individual skyrmions with a high probability of 85%, which could be further enhanced by fabricating magnetic films with lower defect densities. As expected, the higher the sweeping speed, the lower the trapping probability, because the decline in trapping probability at higher sweeping speeds is attributed to skyrmion inertia, which hinders immediate coupling with the dynamic potential of the optical tweezer.

The transport of skyrmions controlled by the photothermal tweezer can be understood as a thermally activated hopping process between intrinsic pinning sites in the magnetic film. The photothermal
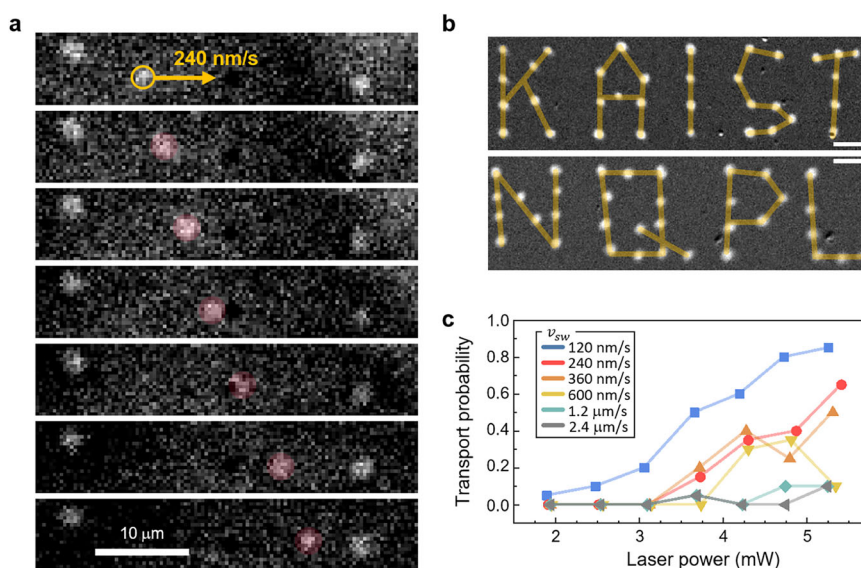

Fig. 2 | Transport and arrangement of individual magnetic skyrmions using the photothermal tweezer. a Photothermal tweezing of an isolated single magnetic skyrmion (colored in red). **b** On-demand arrangement of skyrmions by a photothermal tweezer forming the patterns "KAIST" (upper panel) and "NQPL" (lower panel). Scale bar, 10 µm. **c** Probability of successfully transporting a single skyrmion over a 10 µm distance as a function of the incident laser power and sweeping speed v_{sw}, based on 20 trials for each condition.

potential with a sufficiently strong driving force enables the skyrmion to overcome pinning potentials without deformation, but the probabilistic nature of creep motion determines the success of these "jumps," which depends on the driving duration. If the sweeping speed is too high, skyrmions do not have sufficient time to jump and follow the laser beam. The maximum sweeping speed allowable for jumps with the desired transport probability is inversely proportional to the probabilistic activation time, which follows the Arrhenius equation: $v_{sw} \propto \exp\left(-\frac{E_b}{k_B(T_0 + \alpha P)}\right)$, where E_b is the activation energy barrier, k_B is the Boltzmann constant, P is the laser power, α is the heating coefficient, and T_0 is the ambient temperature. The results in Fig. 2c provide approximate but compelling support for this interpretation (Supplementary Note 6). We note that, beyond this stochastic regime, the skyrmion velocity is ultimately bounded by two factors: a practical limit, determined by the maximum anisotropy gradient and local pinning density (Supplementary Note 3), and a fundamental limit, set by the magnon group velocity[62,63]. Under our current experimental conditions, however, the skyrmion speed is governed primarily by local pinning.

We also demonstrate that the photothermal potential well can pin a selected skyrmion at a desired position, preventing displacement under external electric current injection. We tracked the motion of several skyrmions under electric current pulse injection (Fig. 3a): free

skyrmions (colored blue, yellow, and orange), a skyrmion pinned at a persistent intrinsic defect (colored green), and a selected skyrmion trapped by the photothermal tweezer (colored red). While all free skyrmions move along the direction of the injected current pulses, the photothermally trapped skyrmion, confined by a 6.5 mW laser, remains stationary, similar to the skyrmion pinned at the defect site. The displacement of the skyrmions from their initial positions is shown in Fig. 3b. While the laser for the photothermal potential was on, for the first five current pulses ($N = 0-5$), the displacement of both the photothermally pinned and defect-pinned skyrmions was minimal. By contrast, free skyrmions moved 2.4 μm per pulse on average. We turned off the laser before applying the sixth pulse ($N = 6$), after which the previously photothermally pinned skyrmion started to move freely, while the defect-pinned skyrmion remained stationary. Here, the applied electric pulses were square-shaped with 7.79×10^9 A/m² current density and 100 ms duration.

Higher laser power enhances the depth of the photothermal potential well, thereby increasing the skyrmion resistance to external driving current. We statistically analyzed the displacement of a skyrmion induced by a single electric pulse depending on the laser power and the current density. Figure 3c shows box plots of the first and third quartiles, along with the median, based on 20 trials per condition. To minimize inhomogeneous spatial variations in intrinsic pinning, all measurements were performed on skyrmions at the same location (for further details, see the "Methods" section). Skyrmion transport under current pulses exhibits a threshold behavior, in which the total pinning potential, the sum of the intrinsic and photothermal potentials, must be overcome. Without laser pinning, skyrmions remain pinned unless the current density exceeds a threshold of 4.24×10^9 A/m² (blue dashed line). When the laser pinning is turned on, the additional photothermal potential well increases the threshold current density required for skyrmion motion to 4.56×10^9 A/m² at a laser power of 4.14 mW (orange dashed line) and to over 5.19×10^9 A/m² at 5.06 mW. This result demonstrates the capability of the photothermal effect to locally engineer the potential landscape for skyrmions, offering precise control over their dynamics. Finally, we confirmed the stability of the skyrmion topology under both elevated uniform temperatures and localized photothermal gradients by examining spin–orbit torque-driven transport (Supplementary Note 7).

Fully programmable skyrmion manipulation

The photothermal effect enables the deterministic creation of an isolated skyrmion at a desired position. Localized heating from the focused laser beam reduces the material's magnetic properties, including magnetization and coercivity, and lowers the energy barrier for magnetization reversal (Supplementary Note 8). The flipped magnetization is stabilized by the stray field from neighboring magnetizations[64]. The resulting bubble domain adopts a skyrmionic texture, because the equilibrium state of DWs in our sample is chiral[65,66]. The process of optical skyrmion generation is shown in Fig. 4a. The initial state of the uniformly magnetized domain is shown in the first panel, with the red circle indicating the position of the laser beam in advance. The deterministic creation of a single skyrmion at the irradiated location is shown in the second panel. The generated skyrmion has the same size and shape as the original skyrmions and, as shown in the third panel of Fig. 4a, it exhibits identical motion when we applied an electric pulse (3.14×10^9 A/m² current density and 100 ms duration). Next, the skyrmion Hall effect for optically created skyrmions was measured, confirming their deflection from the direction of the injected current pulse and validating their topological nature and nonzero winding number (Supplementary Note 4).

The probability of skyrmion generation as a function of the incident laser power is shown in Fig. 4b. The laser was applied for 1 s, and the probability was evaluated over 20 trials at different locations for each power level. Below 3 mW, no skyrmions were generated, whereas
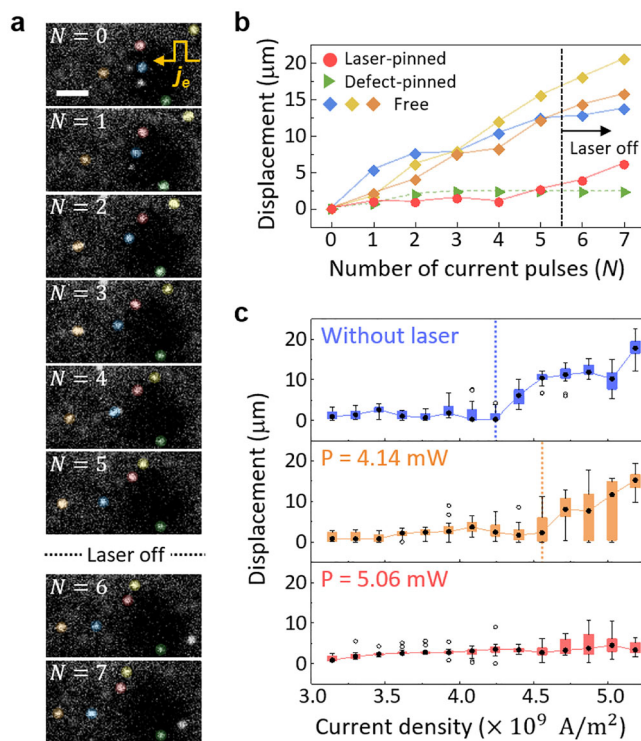
Fig. 3 | Selective photothermal pinning of a magnetic skyrmion. a Snapshots of magnetic skyrmions under successive electric current pulses. N denotes the number of current pulses applied from the initial state ($N = 0$). Individual skyrmions are highlighted in different colors for clarity: the red-shaded skyrmion was photothermally pinned, the green-shaded skyrmion was pinned at an intrinsic defect site, and the other skyrmions were free to move under electric current pulses. Scale bar, 10 μm. **b** Displacements of the skyrmions shown in (**a**) as a function of the number of applied current pulses. The pinning laser was turned off between the fifth and sixth pulses. **c** Statistical analysis of skyrmion displacement induced by a single current pulse, with and without laser pinning ($P = 4.14$ mW and 5.06 mW). The data from 20 trials per condition are presented by box plots, showing the first and third quartiles, the median as a solid dot, and outliers as empty circles outside the 1.5 interquartile range.
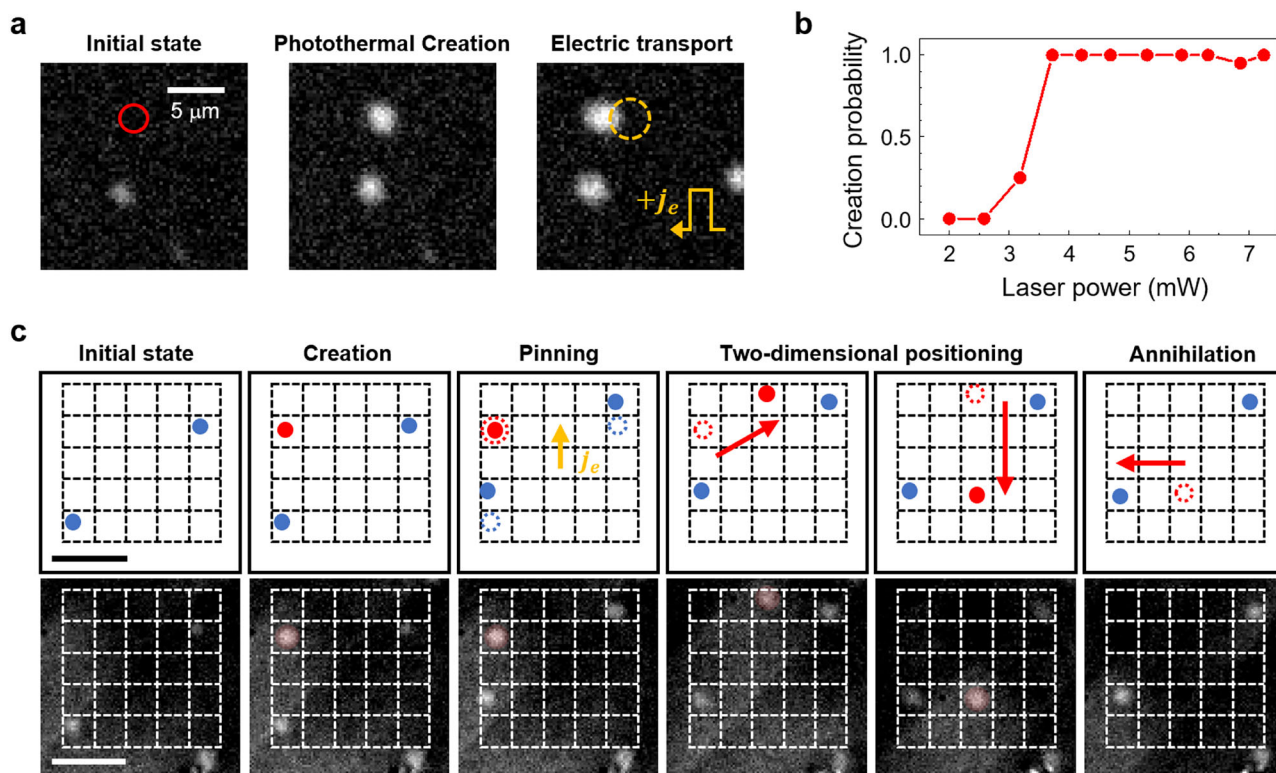
Fig. 4 | Fully programmable control of a magnetic skyrmion using a photothermal tweezer. a Photothermal creation of a skyrmion and its subsequent electrical drift. **b** Probability of skyrmion creation as a function of the incident laser power. **c** Programmed skyrmion motion under successive operation based on the photothermal tweezer, including its creation, pinning, positioning, and annihilation. Scale bar, 10 μm.

above 4 mW, the skyrmion formation probability increased dramatically, ultimately reaching deterministic creation. This result demonstrates that photothermal skyrmion generation requires a laser power exceeding a certain threshold, and it can be explained with an Arrhenius equation (see supplementary Note 8 for details). Conventional skyrmion creation methods using external magnetic fields[65,66], ultrafast lasers[51,52], and electrical current pulses[64], are limited to either generating a large number of skyrmions stochastically or restricting their formation to predefined locations such as electrodes or tracks. By contrast, photothermal generation enables precise and deterministic skyrmion creation at arbitrary positions, making it a versatile tool for potential quantum and spintronic applications. Furthermore, at sufficiently high laser power, two skyrmions can be induced to merge into a single skyrmion, enabling selective annihilation (Supplementary Note 9).

By integrating the techniques outlined above, we demonstrated fully programmable control over the motion of an individual skyrmion through successive operations of the photothermal tweezer. As shown in Fig. 4c, the comprehensive manipulation, including skyrmion creation, pinning, transport, and annihilation, within a 5 × 5 cell array was experimentally demonstrated. Each unit cell measures 4.3 μm × 4.3 μm, a spacing determined by the typical displacement of a skyrmion induced by an electrical pulse (3.14×10^9 A/m² current density and 100 ms duration). Starting from an initial configuration with two preexisting skyrmions (colored blue), and using the photothermal effects, a new skyrmion (colored red) was created at a target position. The created skyrmion was pinned with a photothermal tweezer, whereas the two preexisting skyrmions were shifted by an electric pulse. Subsequently, the created skyrmion was transported independently to other cells using the photothermal tweezer. Unlike electrical current-driven motion, which is restricted to predetermined directions, the photothermal tweezer enables flexible two-dimensional skyrmion positioning with high spatial precision.

Finally, the created skyrmion was dragged to a preexisting skyrmion, and as they approached closer, the DWs separating them became demagnetized by the thermal effect. This operation provided enough energy to break the topological barrier, merging them into a single skyrmion. The ability to control the birth, movement, and annihilation of individual skyrmions shows the potential of advanced two-dimensional spintronic application[67,68].

Discussion

In this study, we demonstrated the optical manipulation of skyrmions, magnetic quasiparticles, using a micrometer-scale photothermal potential well generated by a focused laser beam. The photothermal potential, which effectively attracts magnetic chiral DWs, enables precise tweezing and pinning of an individual skyrmion at a desired position, even overcoming transport driven by electric current injection. The properties and performance of the photothermal skyrmion tweezer, as a function of incident laser power and sweeping speed, were quantitatively investigated. The photothermal effect can also create or annihilate a single skyrmion. By combining collective electric transport for large-scale skyrmion motion with targeted photothermal manipulation of selected skyrmions, we achieved efficient, fully programmable two-dimensional manipulation. The concept of photothermal tweezers may also be extended to other magnetic quasiparticles, such as hopfions, antiskyrmions, and merons, as their magnetic ordering decreases upon heating in a manner similar to skyrmions. Furthermore, advances in wavefront engineering with spatial light modulators could enable photothermal tweezers with complex configurations such as trap arrays, ratchets, and tailored beam profiles[69] opening opportunities for sophisticated studies of skyrmion interactions and coupling with other spin textures. In particular, holographic photothermal tweezers could provide a powerful platform for studying skyrmion dynamics on engineered periodic or disordered pinning landscapes[47-49]. Finally, the programmable

creation, manipulation, and annihilation of individual skyrmions will expand the functionalities of existing skyrmionic devices, such as probabilistic computing architectures, multiplexers, and reconfigurable logic gates.

Methods

Sample fabrication

The magnetic thin films, consisting of an MgO (1 nm) / Ta (0.1 nm) / $Co_{20}Fe_{60}B_{20}$ (1.2 nm) / W (3 nm) / TaO_x (3 nm) stack, were deposited on a Si/SiO_2 substrate by DC/RF magnetron sputtering. After deposition, the sample underwent a post-annealing process at 350 °C for 1 h under a 1×10^{-7} Torr vacuum. For electrical transport measurements of magnetic skyrmions, electrodes composed of Ti (2 nm) / Au (50 nm) were fabricated using photo-lithography and a lift-off process. We prepared two identical samples grown under the same fabrication conditions. Sample #1 was used for the experiments shown in Fig. 2a, c, as well as Fig. 3a, b, while Sample #2 was used for those in Fig. 2b, Fig. 3c, and Fig. 4. This separation was intended to avoid inaccuracies due to potential sample degradation from repeated experiments used for statistical analysis. We confirmed the equivalence of the magnetic properties of the two samples (see Supplementary Note 1 for more details).

Experimental setup

Local photothermal heating was achieved using a focused 638 nm continuous-wave (CW) laser. The diameter of the focused laser beam was 2.4 μm, comparable to the typical skyrmion size in the magnetic films studied. The magneto-optical Kerr effect (MOKE) microscopy setup for real-time skyrmion motion measurements consisted of a 530 nm light-emitting diode (LED) for illumination and an electron-multiplying charge-coupled device (iXon DU-897). A piezoelectric translation stage was used to precisely move the sample in two dimensions, allowing the focused beam to sweep relative to the sample. Custom-built electromagnets were used to apply both in-plane and out-of-plane magnetic fields simultaneously. For all experiments shown in the main manuscript, an out-of-plane magnetic field of 2.56 Oe was applied to tune skyrmion size. An in-plane magnetic field was applied only during the initial nucleation of skyrmions from the stripe domain state across the sample and was then set to zero during all other measurements.

Photothermal pinning measurement

For statistical analysis of the motion of photothermally pinned skyrmions per electrical current pulse (Fig. 3c in the main text), we examined skyrmions created at the same predefined position and minimized differences arising from spatial inhomogeneity across the sample. The photothermal effect enabled the deterministic creation of a skyrmion at a fixed position, carefully selected to avoid any persistent intrinsic defects that might skew the statistical results. Instances where the target skyrmion was annihilated by high-current-density electrical pulses were excluded from the statistical analysis. The motion of skyrmions was tracked in real time using the MOKE microscope and quantitatively analyzed using the TrackMate plugin in ImageJ software (National Institutes of Health and the Laboratory for Optical and Computational Instrumentation, University of Wisconsin).

Data availability

The data that support the findings of this study are available from the corresponding author upon reasonable request.

References

1. Je, S.-G. et al. Direct demonstration of topological stability of magnetic skyrmions via topology manipulation. *ACS Nano* **14**, 3251–3258 (2020).
2. Wang, K., Bheemarasetty, V., Duan, J., Zhou, S. & Xiao, G. Fundamental physics and applications of skyrmion: a review. *J. Magn. Magn. Mater.* **563**, 169905 (2022).
3. Yu, G. et al. Room-temperature skyrmion shift device for memory application. *Nano Lett.* **17**, 261–268 (2017).
4. Luo, S. et al. Reconfigurable skyrmion logic gates. *Nano Lett.* **18**, 1180–1184 (2018).
5. Zázvorka, J. et al. Thermal skyrmion diffusion used in a reshuffler device. *Nat. Nanotechnol.* **14**, 658–661 (2019).
6. Song, K. M. et al. Skyrmion-based artificial synapses for neuromorphic computing. *Nat. Electron.* **3**, 148–155 (2020).
7. Beneke, G. et al. Gesture recognition with Brownian reservoir computing using geometrically confined skyrmion dynamics. *Nat. Commun.* **15**, 8103 (2024).
8. Yokouchi, T. et al. Pattern recognition with neuromorphic computing using magnetic field-induced dynamics of skyrmions. *Sci. Adv.* **8**, eabq5652 (2022).
9. Litzius, K. et al. Skyrmion Hall effect revealed by direct time-resolved X-ray microscopy. *Nat. Phys.* **13**, 170–175 (2017).
10. Jiang, W. et al. Direct observation of the skyrmion Hall effect. *Nat. Phys.* **13**, 162–169 (2017).
11. Kurumaji, T. et al. Skyrmion lattice with a giant topological Hall effect in a frustrated triangular-lattice magnet. *Science* **365**, 914–918 (2019).
12. Shao, Q. et al. Topological Hall effect at above room temperature in heterostructures composed of a magnetic insulator and a heavy metal. *Nat. Electron.* **2**, 182–186 (2019).
13. Hirata, Y. et al. Vanishing skyrmion Hall effect at the angular momentum compensation temperature of a ferrimagnet. *Nat. Nanotechnol.* **14**, 232–236 (2019).
14. Pham, V. T. et al. Fast current-induced skyrmion motion in synthetic antiferromagnets. *Science* **384**, 307–312 (2024).
15. Dai, B. et al. Electric field manipulation of spin chirality and skyrmion dynamic. *Sci. Adv.* **9**, eade6836 (2023).
16. Maccariello, D. et al. Electrical detection of single magnetic skyrmions in metallic multilayers at room temperature. *Nat. Nanotechnol.* **13**, 233–237 (2018).
17. Zheng, F. et al. Skyrmion–antiskyrmion pair creation and annihilation in a cubic chiral magnet. *Nat. Phys.* **18**, 863–868 (2022).
18. Du, H. et al. Interaction of individual skyrmions in a nanostructured cubic chiral magnet. *Phys. Rev. Lett.* **120**, 197203 (2018).
19. Weber, T. et al. Topological magnon band structure of emergent Landau levels in a skyrmion lattice. *Science* **375**, 1025–1030 (2022).
20. Mochizuki, M. et al. Thermally driven ratchet motion of a skyrmion microcrystal and topological magnon Hall effect. *Nat. Mater.* **13**, 241–246 (2014).
21. Kato, Y. D., Okamura, Y., Hirschberger, M., Tokura, Y. & Takahashi, Y. Topological magneto-optical effect from skyrmion lattice. *Nat. Commun.* **14**, 5416 (2023).
22. Vélez, S. et al. Current-driven dynamics and ratchet effect of skyrmion bubbles in a ferrimagnetic insulator. *Nat. Nanotechnol.* **17**, 834–841 (2022).
23. Ji, Y. et al. Direct observation of room-temperature magnetic skyrmion motion driven by ultra-low current density in van der Waals ferromagnets. *Adv. Mater.* **36**, 2312013 (2024).
24. Song, M. et al. Universal hopping motion protected by structural topology. *Adv. Mater.* **34**, 2203275 (2022).
25. Peng, L. et al. Dynamic transition of current-driven single-skyrmion motion in a room-temperature chiral-lattice magnet. *Nat. Commun.* **12**, 6797 (2021).
26. Chen, R. et al. Ordered creation and motion of skyrmions with surface acoustic wave. *Nat. Commun.* **14**, 4427 (2023).
27. Yu, X. et al. Real-space observations of 60-nm skyrmion dynamics in an insulating magnet under low heat flow. *Nat. Commun.* **12**, 5079 (2021).

28. Qin, G. et al. Dynamics of magnetic skyrmions driven by a temperature gradient in a chiral magnet FeGe. *Phys. Rev. B* **106**, 024415 (2022).

29. Casiraghi, A. Individual skyrmion manipulation by local magnetic field gradients. *Commun. Phys.* **2**, 145 (2019).

30. Ashkin, A., Dziedzic, J. M., Bjorkholm, J. E. & Chu, S. Observation of a single-beam gradient force optical trap for dielectric particles. *Opt. Lett.* **11**, 288–290 (1986).

31. Ashkin, A. History of optical trapping and manipulation of small-neutral particle, atoms, and molecules. *IEEE J. Sel. Top. Quantum Electron.* **6**, 841–856 (2000).

32. Curtis, J. E., Koss, B. A. & Grier, D. G. Dynamic holographic optical tweezers. *Opt. Commun.* **207**, 169–175 (2002).

33. Black, J. W., Kamenetska, M. & Ganim, Z. An optical tweezers platform for single molecule force spectroscopy in organic solvents. *Nano Lett.* **17**, 6598–6605 (2017).

34. Wang, X. et al. Enhanced cell sorting and manipulation with combined optical tweezer and microfluidic chip technologies. *Lab Chip* **11**, 3656–3662 (2011).

35. Schlosser, N., Reymond, G., Protsenko, I. & Grangier, P. Sub-poissonian loading of single atoms in a microscopic dipole trap. *Nature* **411**, 1024–1027 (2001).

36. Kim, H. et al. In situ single-atom array synthesis using dynamic holographic optical tweezers. *Nat. Commun.* **7**, 13317 (2016).

37. Bustamante, C. J., Chemla, Y. R., Liu, S. & Wang, M. D. Optical tweezers in single-molecule biophysics. *Nat. Rev. Methods Prim.* **1**, 25 (2021).

38. Liu, L. R. et al. Building one molecule from a reservoir of two atoms. *Science* **360**, 900–903 (2018).

39. Shadmany, D. et al. Cavity QED in a high NA resonator. *Sci. Adv.* **11**, eads8171 (2025).

40. Holland, C. M., Lu, Y. & Cheuk, L. W. On-demand entanglement of molecules in a reconfigurable optical tweezer array. *Science* **382**, 1143–1147 (2023).

41. Cheuk, L. W. et al. Observation of collisions between two ultracold ground-state CaF molecules. *Phys. Rev. Lett.* **125**, 043401 (2020).

42. Ebadi, S. et al. Quantum phases of matter on a 256-atom programmable quantum simulator. *Nature* **595**, 227–232 (2021).

43. Bornet, G. et al. Scalable spin squeezing in a dipolar Rydberg atom array. *Nature* **621**, 728–733 (2023).

44. Ogawa, N. et al. Photodrive of magnetic bubbles via magnetoelastic waves. *Proc. Natl Acad. Sci. USA* **112**, 8977–8981 (2015).

45. Veshchunov, I. S. et al. Optical manipulation of single flux quanta. *Nat. Commun.* **7**, 12801 (2016).

46. Wang, X. G. et al. The optical tweezer of skyrmions. *npj Comput. Mater* **6**, 140 (2020).

47. Reichhardt, C. & Reichhardt, C. J. O. Dynamics and nonmonotonic drag for individually driven skyrmions. *Phys. Rev. B* **104**, 064441 (2021).

48. Reichhardt, C. & Reichhardt, C. J. O. Commensuration effects on skyrmion Hall angle and drag for manipulation of skyrmions on two-dimensional periodic substrates. *Phys. Rev. B* **105**, 214437 (2022).

49. Reichhardt, C., Reichhardt, C. J. O. & Milošević, M. V. Statics and dynamics of skyrmions interacting with disorder and nanostructures. *Rev. Mod. Phys.* **94**, 035005 (2022).

50. Fujita, H. & Sato, M. Ultrafast generation of skyrmionic defects with vortex beams: Printing laser profiles on magnets. *Phys. Rev. B* **95**, 054421 (2017).

51. Khela, M. et al. Laser-induced topological spin switching in a 2D van der Waals magnet. *Nat. Commun.* **14**, 1378 (2023).

52. Je, S.-G. et al. Creation of magnetic skyrmion bubble lattices by ultrafast laser in ultrathin films. *Nano Lett.* **18**, 7362–7371 (2018).

53. Gross, I. et al. Direct measurement of interfacial Dzyaloshinskii-Moriya interaction in X|CoFeB|MgO heterostructures with a scanning NV magnetometer (X =Ta,TaN, and W). *Phys. Rev. B* **94**, 064413 (2016).

54. Yang, S. et al. Magnetic skyrmion transistor gated with voltage-controlled magnetic anisotropy. *Adv. Mater.* **35**, 2208881 (2023).

55. Chikazumi, S. *Physics of Ferromagnetism* (Oxford Univ. Press, 2009).

56. Lee, K.-M., Choi, J. W., Sok, J. & Min, B.-C. Temperature dependence of the interfacial magnetic anisotropy in W/CoFeB/MgO. *AIP Adv.* **7**, 065107 (2017).

57. Schlotter, S. et al. Temperature dependence of the Dzyaloshinskii-Moriya interaction in Pt/Co/Cu thin film heterostructures. *Appl. Phys. Lett.* **113**, 092402 (2018).

58. Moretti, S., Raposo, V., Martinez, E. & Lopez-Diaz, L. Domain wall motion by localized temperature gradients. *Phys. Rev. B* **95**, 064419 (2017).

59. Schlickeiser, F., Ritzmann, U., Hinzke, D. & Nowak, U. Role of entropy in domain wall motion in thermal gradients. *Phys. Rev. Lett.* **113**, 097201 (2014).

60. Jena, J. et al. Observation of fractional spin textures in a Heusler material. *Nat. Commun.* **13**, 2348 (2022).

61. Yang, S. et al. Control of the half-skyrmion Hall effect and its application to adder-subtractor. *Adv. Quantum Technol.* **4**, 2000060 (2021).

62. Caretta, L. et al. Relativistic kinematics of a magnetic soliton. *Science* **370**, 1438–1442 (2020).

63. How, H., O'Handley, R. C. & Morgenthaler, F. R. Soliton theory for realistic magnetic domain-wall dynamics. *Phys. Rev. B* **40**, 4808–4817 (1989).

64. Yang, S. et al. Electrical generation and deletion of magnetic skyrmion-bubbles via vertical current injection. *Adv. Mater.* **33**, 2104406 (2021).

65. Moon, K.-W. et al. Universal method for magnetic skyrmion bubble generation by controlling the stripe domain instability. *NPG Asia Mater.* **13**, 20 (2021).

66. Yang, S. et al. Magnetic field magnitudes needed for skyrmion generation in a general perpendicular magnetized film. *Nano Lett.* **22**, 8430–8436 (2022).

67. Zhang, X. et al. Configurable pixelated skyrmions on nanoscale magnetic grids. *Commun., Phys.* **4**, 255 (2021).

68. Xia, J. et al. Transformation of a cellular skyrmion to polyomino-like structures. *Appl. Phys. Lett.* **125**, 032404 (2024).

69. Grier, D. G. A revolution in optical manipulation. *Nature* **424**, 810–816 (2003).

Acknowledgements

Author contributions

J.K. and M.K.S. conceived the project. S.Y. and K.W. fabricated the sample. J.K. performed all the measurements and analysis. J.K., S.Y., and M.K.S. analyzed the data. J.K. and M.K.S. wrote the manuscript with the assistance of C.H., D.K., C.K., and all other authors.

Competing interests

The authors declare no competing interests

Additional information